NIH Public Access
Author Manuscript
J Phys Chem B. Author manuscript; available in PMC 2012 October 01.

Published in final edited form as:
J Phys Chem B. 2011 June 23; 115(24): 7830–7837. doi:10.1021/jp2020148.

A coarse-grained model for PEGylated lipids: the effect of PEGylation on size and shape of self-assembled structures

Hwankyu Lee[1,2,*] and **Richard W. Pastor**[2]

[1]Department of Chemical Engineering, Dankook University, Yongin, 448-701, South Korea

[2]Laboratory of Computational Biology, National Heart, Lung, and Blood Institute, National Institutes of Health, Bethesda, MD 20892, USA

Abstract

Self-assembly of polyethylene glycol (PEG)-grafted lipids at different sizes and concentrations was simulated using the MARTINI coarse-grained (CG) force field. The interactions between CG PEG and CG dipalmitoylglycerophosphocholine (DPPC)-lipids were parametrized by matching densities of 19-mers of PEG and polyethylene oxide (PEO) grafted to the bilayer from all-atom simulations. Mixtures of lipids and PEG(M_w = 550, 1250, 2000)-grafted lipids in water self-assembled to liposomes, bicelles, and micelles at different ratios of lipids and PEGylated lipids. Average aggregate sizes decrease with increasing PEGylated-lipid concentration, in qualitative agreement with experiment. PEGylated lipids concentrate at the rims of bicelles, rather than at the planar surfaces; this also agrees with experiment, though the degree of segregation is less than that assumed in previous modeling of the experimental data. Charged lipids without PEG evenly distribute at the rim and planar surface of the bicelle. The average end-to-end distances of the PEG on the PEGylated lipids are comparable in liposomes, bicelles (edge or planar surface), and micelles, and only slightly larger than for an isolated PEG in solution. The ability of PEGylated lipids to induce the membrane curvature by the bulky head group with larger PEG, and thereby modulate the phase behavior and size of lipid assemblies, arises from their relative concentration.

INTRODUCTION

Liposomes, biodegradable polymers, and nanoparticles show great potential for drug delivery applications, but their poor solubility and short circulating lifetime limit their effectiveness.[1–13] To overcome these difficulties, polyethylene glycol (PEG) or polyethylene oxide (PEO) has been conjugated to drug carriers, a process called PEGylation.[14–17] PEGylated liposomal carriers have been widely used for pharmaceutical applications, and recently PEGylated bicelles and micelles showed potential for drug delivery and biophysical applications. PEGylated micelles carry small hydrophobic drugs,[18] and PEGylated bicelles can be used as model membranes for drug partition studies.[19] To control these different structures of the PEGylated-lipid aggregates, the aggregate structures and their dependence on the concentration and size of PEG need to be understood.

Molecular dynamics (MD) simulations of PEGylated lipids have shown that higher concentration and larger size of PEG induce smaller micelles.[20] Also, the electrostatic and hydrophobic interactions between PEO and charged micelles were studied to understand preference for anionic micelles.[21,22] However, due to system size limitations, only micelles were examined. Coarse-grained (CG) and mesoscale simulations have shown the formation of liposomes and bicelles, although the simulated liposomes are much smaller than those

*Corresponding author, leeh@dankook.ac.kr.

NIH-PA Author Manuscript
NIH-PA Author Manuscript
NIH-PA Author Manuscript

NIH-PA Author Manuscript

NIH-PA Author Manuscript

NIH-PA Author Manuscript

observed from experiment.[23–25] However, a systematic exploration of PEGylation-induced phase behaviors of liposomes, bicelles, and micelles has been limited by the absence of a well-validated CG model of lipid/PEG interaction.

The study involved developing a suitable model of PEG/lipid systems, testing it, and analyzing the effects of grafted PEG on the curvature of lipid assemblies. The development strategy was similar to that employed to obtain CG parameters for PEG/water solutions[26] within the framework of the MARTINI CG lipid force field (FF).[27,28] All-atom simulations of 19-mers of PEG and 18-mers of PEO grafted to a lipid bilayer were carried out to yield density distributions of the polymers with respect to the bilayer surface. The Lennard-Jones (LJ) terms for monomer/lipid interaction in the MARTINI FF were then modified so that CG simulations of the same systems yielded similar distributions. Testing involved using the CG FF for simulating self-assemblies of mixtures of lipids and PEGylated lipids with various PEG sizes and PEGylated concentrations, and comparing the phase with experiment.

METHODS

All-atom simulations of PEG grafted on lipid bilayer

Simulations and analyses were performed with the CHARMM simulation package (c35b1).[29] The CHARMM ether parameters (C35r)[30,31] and lipid parameters (C36)[32] were used for PEG and lipids. 19-mers of PEG and 18-mers of PEO have equivalent molecular weight of ~840, and simulations were performed for each. The simulated bilayer consists of 128 dipalmitoylglycerophosphocholine (DPPC) lipids (64 DPPC/leaflet), 19-mers of PEG (or 18-mers of PEO), and ~18000 water molecules in the simulation box of size 63 × 63 × 180 $Å^3$ (Figure 1, *top left*). A terminal carbon of PEO (or terminal oxygen of PEG) was linked to a headgroup of DPPC at the center of bilayer by applying a distance constraint of 1.5 Å. Particle mesh Ewald summation[33] and a real space cutoff of 12 Å were applied for electrostatic forces. The LJ forces were switched to zero between 8 Å and 12 Å. The temperature was maintained at 296 K by applying a Nose-Hoover thermostat,[34] and the fixed surface area and constant normal pressure (NP_zAT) were used by applying an Andersen-Hoover barostat;[35,36] the preceding constraints maintained the bilayer in the fluid phase and allowed comparison with useful target data. Simulations were performed for 40 ns with a time step of 2 fs, and the last 30 ns were used for analyses.

Parameterization of the CG model for the PEG-lipid interaction

The potential energy function for CG PEG was previously developed[26] within the framework of the MARTINI CG FF. A monomer of PEG or PEO has three heavy atoms (COC), and each monomer is mapped onto one CG bead. LJ, electrostatic, bond, angle, and torsional terms were parametrized by comparing densities, conformations, and hydrodynamics of differently sized PEG molecules with experimental values. This CG model does not distinguish PEG and PEO (a 19-mer of PEG is equivalent to an 18-mer of PEO). This feature is justified by result that all-atom simulations of 27-mers of PEO and 28-mers of PEG in water yield very similar end-to-end distance distributions.[26] This study required the extension of the CG PEG model to include interactions with DPPC.

Figure 1 shows structures of DPPC, PEGylated, and charged lipids. To model PEGylation, the terminal CG bead of the 45-mers of PEG (M_w = ~2000) was attached to the head group of a DPPC, and the CG bead “Q0” (+1 charge) for the DPPC choline was converted to the bead type “P4” (no charge; polar) to represent the amide group of the linkage between PEG and lipid, leading to a net charge of −1 for the PEGylated lipid. The CG amide and PEG beads were linked with the bond and angle potentials, as described in our previous work.[26] Since mixtures of DPPC and PEGylated dipalmitoylglycerophosphoethanolamine (DPPE)

NIH-PA Author Manuscript

NIH-PA Author Manuscript

NIH-PA Author Manuscript

are studied in experiments, this PEGylated lipid is denoted "DPPE-PEG45". 12- and 28-mers of PEG (M_w = ~550 and ~1250) were also attached to DPPE and named "DPPE-PEG12" and "DPPE-PEG28", respectively. Experimentally, larger PEG chains (M_w = 5000) have been also applied, but they were not simulated here, which requires much larger system size. To isolate the effects of head group size and charge, the PEG moiety was removed from a DPPE-PEG; this test lipid has a charge of −1 and is denoted "DPPE-PEG0".

To parametrize the interactions between CG PEG and CG DPPC lipids, all-atom and CG simulations of DPPC bilayers with attachment of 18-mers of PEO or 19-mers of PEG were performed with water. All-atom simulations were performed for both 18-mers of PEO and 19-mers of PEG to determine whether conformations of PEO and PEG on the lipid bilayer are significantly different. The PEG bead is treated as a "SNda" type for the PEG-PEG and PEG-water interactions within the framework of the MARTINI CG FF, which uses σ_{ij} = 4.3 Å and ε_{ij} = 3.375 kJ/mol for the LJ potential. As the first step of parameterization, the SNda type of PEG was applied for the PEG-DPPC interaction, where the MARTINI CG FF produces the LJ potentials of σ_{ij} = 4.7 and ε_{ij} = 4.0 for PEG-choline; σij = 4.7 and ε_{ij} = 5.0 for PEG-phosphate; σ_{ij} = 4.7 and ε_{ij}= 4.5 for PEG-glycerol. These parameters resulted in strong adsorption of PEG molecules onto the bilayer surface. Similar strong adsorption was also observed in CG simulations by Srinivas and Klein.[37] In contrast, all-atom simulations of PEG and PEO show no adsorption onto lipid bilayers (Figure 2, *top left* and *bottom*), in agreement with experimental studies.[38,39] Essentially, PEG adapts solution-like conformations consistent with the "mushroom" state of grafted polymers at low concentration.[40] These results indicate that a SNda type is too strong for the interaction between PEG and DPPC bilayers. Therefore, the weaker CG bead type of PEG, "N0", is applied only for the PEG-DPPC interaction, where the MARTINI CG FF produces less attractive LJ potentials of σ_{ij} = 4.7 and ε_{ij} = 3.5 for PEG-choline, PEG-phosphate, and PEG-glycerol interactions. Note that although the N0 type of PEG is used for the PEG-DPPC interaction, the SNda type of PEG is still applied for PEG-PEG and PEG-water interactions. With the N0 bead type, CG simulations show no adsorption of PEG onto the lipid bilayer, and the distributions normal to the bilayer surface compare well with those from the all-atom simulations (Figure 2, bottom), favorably compared with the solution-like conformation observed from experiment at low PEGylated-lipid concentration.[38,39] However, the small differences between PEG and PEO from the all-atom simulations (possibly involving interactions of the terminal hydroxyl group of PEG with bilayer surface) cannot be captured by the present PEG/PEO CG model.

CG simulations of PEG grafted on lipid bilayer

Simulations and analyses were performed using the GROMACS4.0.5 simulation package[41,42] with the MARTINI CG lipid[27] and PEG FFs.[26] The simulated bilayer consists of 200 CG DPPC (100 DPPC/leaflet), 2 CG PEG (1 PEG/leaflet) and ~8800 CG water molecules (~35200 real waters) in a periodic box of size 78 × 78 × 227 Å^3 (Figure 2, *top right*). A terminal CG bead of each PEG molecule was linked to a CG bead of the head group of a DPPC lipid located at the center of each leaflet in lipid bilayer by applying a distance constraint with 3.3 Å. For comparison with all-atom simulations, the same temperature of 296 K was maintained by applying a Berendsen thermostat in the NPT ensemble,[43] leading to the equilibrated area per lipid of 61 Å^3, close to those calculated from all-atom simulations with the NP$_z$AT ensemble, as described above. A cutoff of 12 Å was used for the LJ potential and electrostatic interactions. The LJ potential was smoothly shifted to zero between 9 and 12 Å, and the Coulomb potential was smoothly shifted to zero between 0 and 12 Å. Simulations were run for 800 ns with a time step of 8 fs, and the final 500 ns were used for analyses.

NIH-PA Author Manuscript

NIH-PA Author Manuscript

NIH-PA Author Manuscript

CG simulations of self-assembly of PEGylated lipids

The same GROMACS tools, the MARTINI CG PEG and lipid FFs, and simulation parameters were used as described above. The transition temperature for MARTINI DPPC is 295 K,[24,44] which is lower than the experiment value by ~20 K. Also, it has been experimentally known that smaller liposomes have the lower transition temperature (~310 K and ~314 K respectively for <35 nm and >75 nm in diameter of the liposome).[45] Therefore, the fixed simulation temperature of 296 K, which is used for most experiment measurements, was applied for better comparison with experiments, although only qualitative comparison for phase behaviors can be achieved.

Mixtures of DPPC and DPPE-PEG were simulated in water at concentrations of 0, 2.2, 10.5, 27.4, and 99 mol% DPPE-PEG12, -PEG28, and -PEG45 (Table 1). For the system at the concentration of 0 mol% DPPE-PEG, 10500 DPPC lipids were randomly distributed in the simulation box of 400 Å/side, and then ~400000 CG water molecules (representing ~1600000 real waters) were added, leading to the final lipid concentration of ~280 mM. Although the concentration of 280 mM is much higher than the experiment concentration of ~10 mM, such a high concentration is necessary to simulate self-assembly of liposomes with available computer time. The total number (10500) of lipids was constant for all DPPC/DPPE-PEG mixtures at the DPPE-PEG concentrations of 0, 2.2, 10.5, and 27.4 mol%. To maintain the lipid concentration of ~280 mM and the system volume with 400 Å/side, systems with higher concentrations and larger sizes of PEG included less water molecules. For 99mol% DPPE-PEG, 3000 lipids and 43000 water beads were distributed in the simulation box of 260 Å/side. To neutralize the system, 231, 1100, 2875, and 2970 NA^+ counterions were added to systems with 2.2, 10.5, 27.4, and 99 mol% PEG, respectively. 3–5 simulations for each system were performed for 300 ns, and the last 100 ns was used for analyses.

RESULTS

Dependence of phase behavior on concentration and size of PEGylated lipids

Mixtures of DPPC and DPPE-PEG were simulated in water with different sizes and concentrations of PEG (Table 1). They spontaneously self-assembled to liposomes, bicelles, micelles, or their mixtures within 300 ns; Figure 3 shows the initial (*far left*) and final snapshots for systems with 0–99 mol% DPPE-PEG45. Liposomes with outer diameters of 220–320 Å formed at concentrations of 0 and 2.2 mol% DPPE-PEG45. While PEGylated lipids are located on both surfaces of the liposome, not surprisingly they are more concentrated on the outer surface. An asymmetric distribution allows formation of small liposomes without the crowding problems of PEG chains grafted to the inner layer. This is quantitated for the systems at 2.2 mol% DPPE-PEG45 in Table 2. DPPE-PEG45 concentration is 2.0–2.5 mol% at the outer layer of the liposome, and 1.1–1.5 mol% at the inner layer, and ratios of lipids (1.62:1 to 1.37:1) decreases as liposome size increases. The area per lipid ranges 64–67 $Å^2$ in the outer and inner layers; i.e., they are all in the fluid state, as consistent with the phase transition temperature of the MARTINI model for DPPC. These simulated liposomes are smaller than the experimentally observed sizes of >100 nm at 25 °C,[46] and closer to sonicated DPPC vesicles at 20 °C (~20 nm).[47] Small fragments such as micelles were not detected in experiment up to 5–10 mol% DPPE-PEG;[46] they form in the simulation because the remaining lipids are not sufficient to form another liposome. Bicelles and micelles are observed in the simulation at 10.5 mol%, and these decrease in size at 27.4 mol%; only small micelles are present at 99.0 mol% DPPE-PEG45. Note that in experiment the bicelles were observed only by heating the sample above the transition temperature and then cooling down to room temperature,[48] while they form spontaneously in the simulation. Although differences in methodology, system size, and aggregate sizes

NIH-PA Author Manuscript

NIH-PA Author Manuscript

NIH-PA Author Manuscript

preclude quantitative comparisons, the trend for the preceding phase behavior agrees with experiment, where liposomes stably form up to 5~10 mol% DPPE-PEG45, bicelles start to form at ~10 mol%, and there are only small micelles at concentrations of more than 30–35 mol%.[46,49] Although the PEGylated-lipid concentrations in simulation are not exactly same as those in experiment, 10.5 and 27.4 mol% from simulation are close to the boundaries of the experimental data, 10 and 30 mol%. Note that in experiment these phase transitions occur smoothly over the broad range of the PEGylated-lipid concentration, and hence these choices of concentrations close to experimental boundaries are reasonable.

Figure 4 plots the distributions of lipids per aggregate for the systems with 2.2, 10.5, and 99.0 mol% DPPE-PEG45. While the distribution is essentially bimodal at 2.2 mol% (a single liposome with ~7400 lipids, and small bicelles and micelles with <300 lipids), a number of differently sized bicelles form at 10.5 mol% (but no liposomes). At 99.0 mol%, aggregated lipid numbers are distributed in the broad range of ~130 or less, which makes it difficult to distinguish between micelles and small bicelles. Similar trends were observed for systems with DPPE-PEG12 and DPPE-PEG28.

Average numbers of lipids per liposome at 2.2 mol% DPPE-PEG0, DPPE-PEG12, DPPE-PEG28, and DPPE-PEG45 were 7116 ± 161, 7219 ± 474, 4522 ± 984, and 4387 ± 703, respectively. Attachment of PEG12 onto DPPE-PEG0 does not influence the aggregation number. PEG28 and PEG45 significantly reduce the aggregation number (smaller liposomes), presumably because the bulky head group with larger PEG induces more membrane curvature.

Table 3 lists the number ($M_n=\frac{\sum M_i N_i}{\sum N_i}$), weight ($M_w=\frac{\sum M_i^2 N_i}{\sum M_i N_i}$), and Z-averages ($M_z=\frac{\sum M_i^3 N_i}{\sum M_i^2 N_i}$), and the size of the largest aggregate (N_{max}) at 10.5 and 27.4 mol% DPPE-PEG (the bicelle and micelle phases). Attachment of PEG12, PEG28, or PEG45 reduces the average numbers of lipids/aggregate by approximately 40% at 10.5 mol%, and the size of the largest aggregate by 60% compared to DPPE-PEG0. Aggregate sizes are smaller at 27.4 mol%, though the size reductions are comparable to those at 10.5 mol%. The reductions are insensitive to the PEG length for this size range.

Distribution of PEGylated lipids in bicelle

This and the following subsection examine some of the assumptions and simplifications contained in the disk model used to interpret experimental scattering data. First, the aspect ratios (AR) of the bicelles, I_z / I_y, where I_z, I_y, and I_x are principal moments of inertia, ordered such that $I_z > I_y > I_x$, were evaluated to determine whether they are indeed disk-like. Figure 5 plots AR for a bicelle in a simulation system at 10.5 mol% DPPE-PEG45. Since lipids were randomly distributed at the initial configuration, AR begins with approximately 1. At ~30 ns, the aggregate starts to form, and AR quickly increases to 3.5, indicating an irregular ellipsoidal shape. AR gradually decreases, and reaches a steady-state value of ~1.1 at around 200 ns, consistent with a nearly circular disk.

Given that the bicelle is well described as a circular disk, the radial distribution of the component lipids may sensibly be evaluated. Figure 6 shows the results. At 10.5 mol% DPPE-PEG12 or DPPE-PEG45 (1st and 2nd columns), mixtures of DPPC and DPPE-PEG are present up to 120–130 Å from the center, indicating that the radius of the bicelle is about 120–130 Å. Although the system includes 10.5 mol% DPPE-PEG, the fraction does not exceed 7 mol% within 80 Å from the center. The fraction rapidly increases to 28 mol% in

NIH-PA Author Manuscript

NIH-PA Author Manuscript

NIH-PA Author Manuscript

100–130 Å, indicating that PEGylated lipids are more concentrated at the rim of the bicelle. At 10.5 mol% DPPE-PEG45, a similar trend of the distribution of PEGylated lipids was observed from simulations with long-range electrostatics, indicating no dependence on the description of electrostatic interactions. At the higher concentration of 27.4 mol% DPPE-PEG (3rd and 4th columns), smaller bicelles with the radius of < 90 Å were observed. The similar trend of the higher concentration of DPPE-PEG at the rim was observed, but the extent of an increase at the rim is higher over 50 mol%. No significant difference between DPPE-PEG12 and DPPE-PEG45 is observed at 10.5 and 27.4 mol%, indicating that these relatively short chains up to PEG45 do not modulate the aggregate structure, although larger ones may do. To isolate the effects of charge, the lipid number and fraction were calculated for a DPPE-PEG0 system. Figure 6 (5th column) shows that fraction of DPPE-PEG0 is evenly distributed over the entire bicelle area. Finally, Figure 7 presents snapshots of a bicelle from the simulation at 10.5 mol% DPPE-PEG45. It is clear that while PEG is located at the edge, there is substantial density in the planar region.

Size of PEG grafted to liposomes, bicelles, and micelles

To investigate environmental effects on the size of PEG, the root mean squared end-to-end distance $<h^2>^{1/2}$ of PEG was evaluated for each system. For the bicelle, PEG chains within a distance of 120 Å from center of mass (COM) of the bicelle were considered to be on the planar surface, and others were considered to be at the edge. Table 4 shows that $<h^2>^{1/2}$ of PEG grafted to liposome (2.2 mol% DPPE-PEG45), bicelle (10.5 mol% DPPE-PEG45), and micelle (99.0% DPPE-PEG45) are close to each other and only slightly larger than for an isolated PEG in water.[26] They do not show the brushlike (or extended) state obtained in previous simulations of PEG on the bilayer at concentrations of 50–100 mol% PEG.

DISCUSSION AND CONCLUSIONS

The interactions between CG PEG and CG lipid were parametrized by comparing conformations of PEG on the lipid bilayer from all-atom and CG simulations. Using this CG model, simulations show that mixtures of lipids and PEGylated lipids self-assemble to liposomes, bicelles, or micelles, with smaller aggregates at higher concentrations of PEGylated lipids. Similarly, experiments have shown that liposomes stably form up to 5~10 mol% DPPE-PEG45, bicelles start to form at ~10 mol%, and there are only small micelles at concentrations of more than 30–35 mol%.[46,49] Although different experimental methods have shown slightly different concentrations for each phase,[48] the simulated assemblies are consistent with these boundaries. Note that in experiment the formation of the bicelles and small liposomes respectively requires temperature change (heating and cooling between the transition temperature), and sonication.[48] While these methodological differences highlight the approximate nature of the CG model, simulations still reproduce the trend for the experimentally observed phase behavior of PEGylated lipids at different concentrations of PEGylated lipids.

Simulations also show that PEGylation causes smaller aggregates for both liposomes and bicelles, but their effects differ. Different lengths of PEG12, PEG28, and PEG45 do not influence the bicelle size, while they do modulate liposome size. This appears to be related to the migration of the PEGylated lipids in the bicelles to the rim, while those in the liposome are distributed uniformly, as discussed below.

Simulated bicelles initially form with irregular ellipsoidal shapes, but equilibrate to circular disks (Fig 5). This disk shape of the bicelle has been proposed[50] and experimentally supported.[51] A higher fraction of DPPE-PEG is observed at the edge than on the planar surface of the bicelle, in qualitative agreement with experimental observations using SANS.[19] For the systems having the same charge density without PEG chains, DPPE-PEG0

NIH-PA Author Manuscript

NIH-PA Author Manuscript

NIH-PA Author Manuscript

are distributed uniformly on the bicelle surface, indicating that the component segregation of lipids at the planar surface and PEGylated lipids at the rim is caused by the PEG-induced bulky head group rather than by the repulsive electrostatic interactions between anionic lipid head groups. End-to-end distances of PEG45 on liposomes, bicelles, and micelles are also close to each other, and approximately 10% larger than obtain in water (Table 4). Hence, the aggregation state does not modulate the conformation of PEG with molecular weight of 2000 or less.

Although the present simulation results qualitatively agree with the experimental observation of the high DPPE-PEG concentration at the rim of bicelle, a substantial presence of PEG remains on the planar region (Figs 6 and 7). The thickness of the PEG layer at the surface of the fully-PEGylated micelle can be calculated using the brush theory for star-shaped polymers.[52] From Vagberg et al.[53]

$$L=\left[N\,l^{1/\nu}\frac{8\,f^{(1-\nu)/2\nu}}{3\nu 4^{1/\nu}}+R_d{}^{1/\nu}\right]^{\nu}-R_d, \quad (1)$$

where L is the thickness of the PEG layer, N is the number monomers per chain (e.g. 45 for PEG45), l is the statistical length of the monomer (equivalent to the bond length of the CG bead, 3.3 Å), ν is the Flory exponent (3/5 for a good solvent), f is the number of grafted chains (76 for the fully PEGylated micelle, as measured by static light scattering),[54] and R_d is the radius of the micelle core (20 Å). The preceding formula yields L= 34 Å for PEG45. From Table 4, this is close to the end-to-end distance ($<h^2>^{1/2}$) of a single PEG45 molecule in water calculated with the present CG model,[26] though somewhat shorter than obtained here for a micelle, and other aggregates. These results imply that PEG45 is not long enough to adapt brush-like conformations on the fully-PEGylated micelle. A brush state of PEG on a bilayer has been observed in simulations[26] (25–100 mol% PEG45) and X-ray diffraction experiments[38] (10mol% PEG45), indicating that the high curvature of the micelle allows the PEG to adapt a disordered state.

Since PEG45 has the same length for different self-assembled structures, the PEG length calculated from Eq. (1) for the fully-PEGylated micelle can be applied for PEG at the edge of the bicelle, as discussed above. However, longer PEG chains must be considered carefully. For example, $<h^2>^{1/2}$ = 56 Å for PEG113 (M_w=5000) in water,[26] while Eq. (1) yields L=66 Å for the PEG113 grafted on the fully PEGylated micelle. The present simulations indicate that the ratio of DPPE-PEG45 to all lipids is 0.28–0.6 at the edge of the bicelle. It will be interesting to see if this result holds for longer PEG113 at the SANS-experiment concentration of 20 mol% DPPE-PEG113,[19] and if Eq. (1) is still applicable to bicelles.

In conclusion, the interactions between CG PEG and CG lipids were parametrized, and mixtures of lipids and PEGylated lipids in water were simulated at different sizes and concentrations of PEGylated lipids. Simulations capture the phase behavior of the self-assembled liposomes, bicelles, and micelles at different concentrations of PEGylated lipids, in qualitative agreement with experiment. PEGylated lipids are more concentrated at the rims of bicelles than at the planar surfaces, in agreement with experiment. However, the bicelle rim is not fully covered by PEG, and segregation is not complete. These findings imply that the bicelle rim should not be modeled as a fully-PEGylated micelle, and that PEGylated lipids in the planar region contribute to the effective hydrodynamic radius of the bicelle. The importance of these effects remains to be determined, and predictions of CG model must be tested both by experiment and more realistic simulations. Charged lipids without PEG evenly distribute at the rim and the planar surfaces of the bicelle, and form bicelles larger than those with PEGylated lipids. These differences are consistent with the

NIH-PA Author Manuscript

NIH-PA Author Manuscript

NIH-PA Author Manuscript

notion that the bulky head groups with larger PEG induce more membrane curvature, which modulate the phase behavior and aggregate size.

Acknowledgments

This research was supported by the Intramural Research Program of the NIH, National Heart, Lung and Blood Institute. This study utilized the high-performance computational capabilities of the CIT Biowulf/LoBoS3 and NHLBI LOBOS clusters at the National Institutes of Health, Bethesda, MD.

References

1. Lasic DD, Needham D. Chem. Rev. 1995; 95:2601–2628.
2. Bartlett DW, Davis ME. Bioconjugate Chemistry. 2007; 18:456–468. [PubMed: 17326672]
3. Bhadra D, Bhadra S, Jain S, Jain NK. Int. J. Pharm. 2003; 257:111–124. [PubMed: 12711167]
4. Imura Y, Nishida M, Matsuzaki K. Biochim. Biophys. Acta-Biomembr. 2007; 1768:2578–2585.
5. Imura Y, Nishida M, Ogawa Y, Takakura Y, Matsuzaki K. Biochim. Biophys. Acta-Biomembr. 2007; 1768:1160–1169.
6. Kim Y, Klutz AM, Jacobson KA. Bioconjugate Chemistry. 2008; 19:1660–1672. [PubMed: 18610944]
7. Kojima C, Toi Y, Harada A, Kono K. Bioconjugate Chemistry. 2007; 18:663–670. [PubMed: 17375896]
8. Kojima C, Toi Y, Harada A, Kono K. Bioconjugate Chemistry. 2008; 19:2280–2284. [PubMed: 18844391]
9. Lai SK, O'Hanlon DE, Harrold S, Man ST, Wang YY, Cone R, Hanes J. Proc. Natl. Acad. Sci. U. S. A. 2007; 104:1482–1487. [PubMed: 17244708]
10. Steinmetz NF, Manchester M. Biomacromolecules. 2009; 10:784–792. [PubMed: 19281149]
11. Wang W, Xiong W, Wan JL, Sun XH, Xu HB, Yang XL. Nanotechnology. 2009; 20
12. Yang H, Morris JJ, Lopina ST. J. Colloid Interface Sci. 2004; 273:148–154. [PubMed: 15051444]
13. Fahmy TM, Fong PM, Park J, Constable T, Saltzman WM. Aaps Journal. 2007; 9:E171–E180. [PubMed: 17614359]
14. Harris JM, Chess RB. Nat. Rev. Drug Discov. 2003; 2:214–221. [PubMed: 12612647]
15. Harris JM, Martin NE, Modi M. Clin. Pharmacokinet. 2001; 40:539–551. [PubMed: 11510630]
16. Delgado C, Francis GE, Fisher D. Critical Reviews in Therapeutic Drug Carrier Systems. 1992; 9:249–304. [PubMed: 1458545]
17. Roberts MJ, Bentley MD, Harris JM. Adv. Drug Deliv. Rev. 2002; 54:459–476. [PubMed: 12052709]
18. Torchilin VP. Pharm. Res. 2007; 24:1–16. [PubMed: 17109211]
19. Lundquist A, Wessman P, Rennie AR, Edwards K. Biochim. Biophys. Acta-Biomembr. 2008; 1778:2210–2216.
20. Despa F, Luo JT, Li J, Duan Y, Lam KS. Phys. Chem. Chem. Phys. 2010; 12:1589–1594. [PubMed: 20126774]
21. Shang BZ, Wang ZW, Larson RG. J. Phys. Chem. B. 2009; 113:15170–15180. [PubMed: 19905021]
22. Shang BZ, Wang ZW, Larson RG. J. Phys. Chem. B. 2008; 112:2888–2900. [PubMed: 18275181]
23. Shinoda W, DeVane R, Klein ML. J. Phys. Chem. B. 2010; 114:6836–6849. [PubMed: 20438090]
24. Risselada HJ, Marrink SJ. Soft Matter. 2009; 5:4531–4541.
25. Risselada HJ, Marrink SJ. Phys. Chem. Chem. Phys. 2009; 11:2056–2067. [PubMed: 19280016]
26. Lee H, de Vries AH, Marrink SJ, Pastor RW. J. Phys. Chem. B. 2009; 113:13186–13194. [PubMed: 19754083]
27. Marrink SJ, de Vries AH, Mark AE. J. Phys. Chem. B. 2004; 108:750–760.
28. Marrink SJ, Risselada HJ, Yefimov S, Tieleman DP, de Vries AH. J. Phys. Chem. B. 2007; 111:7812–7824. [PubMed: 17569554]

NIH-PA Author Manuscript NIH-PA Author Manuscript NIH-PA Author Manuscript

29. Brooks BR, Brooks CL, Mackerell AD, Nilsson L, Petrella RJ, Roux B, Won Y, Archontis G, Bartels C, Boresch S, Caflisch A, Caves L, Cui Q, Dinner AR, Feig M, Fischer S, Gao J, Hodoscek M, Im W, Kuczera K, Lazaridis T, Ma J, Ovchinnikov V, Paci E, Pastor RW, Post CB, Pu JZ, Schaefer M, Tidor B, Venable RM, Woodcock HL, Wu X, Yang W, York DM, Karplus M. Journal of Computational Chemistry. 2009; 30:1545–1614. [PubMed: 19444816]
30. Lee H, Venable RM, MacKerell AD, Pastor RW. Biophys. J. 2008; 95:1590–1599. [PubMed: 18456821]
31. Vorobyov I, Anisimov VM, Greene S, Venable RM, Moser A, Pastor RW, MacKerell AD. Journal of Chemical Theory and Computation. 2007; 3:1120–1133.
32. Klauda JB, Venable RM, Freites JA, O'Connor JW, Tobias DJ, Mondragon-Ramirez C, Vorobyov I, MacKerell AD, Pastor RW. J. Phys. Chem. B. 2010; 114:7830–7843. [PubMed: 20496934]
33. Darden T, York D, Pedersen L. Journal of Chemical Physics. 1993; 98:10089–10092.
34. Nose S, Klein ML. Journal of Chemical Physics. 1983; 78:6928–6939.
35. Andersen HC. Journal of Chemical Physics. 1980; 72:2384–2393.
36. Hoover WG. Physical Review A. 1985; 31:1695–1697. [PubMed: 9895674]
37. Srinivas G, Klein ML. Molecular Physics. 2004; 102:883–889.
38. Kenworthy AK, Hristova K, Needham D, McIntosh TJ. Biophys. J. 1995; 68:1921–1936. [PubMed: 7612834]
39. Hansen PL, Cohen JA, Podgornik R, Parsegian VA. Biophys. J. 2003; 84:350–355. [PubMed: 12524288]
40. de Gennes PG. Adv. Colloid Interface Sci. 1987; 27:189–209.
41. Hess B, Kutzner C, van der Spoel D, Lindahl E. Journal of Chemical Theory and Computation. 2008; 4:435–447.
42. Lindahl E, Hess B, van der Spoel D. Journal of Molecular Modeling. 2001; 7:306–317.
43. Berendsen HJC, Postma JPM, van Gunsteren WF, DiNola A, Haak JR. Journal of Chemical Physics. 1984; 81:3684–3690.
44. Marrink SJ, Risselada J, Mark AE. Chem. Phys. Lipids. 2005; 135:223–244. [PubMed: 15921980]
45. Koynova R, Caffrey M. Biochim. Biophys. Acta-Rev. Biomembr. 1998; 1376:91–145.
46. Johnsson M, Edwards K. Biophys. J. 2003; 85:3839–3847. [PubMed: 14645073]
47. Cornell BA, Fletcher GC, Middlehurst J, Separovic F. Biochimica Et Biophysica Acta. 1982; 690:15–19. [PubMed: 7126566]
48. Sandstrom MC, Johansson E, Edwards K. Biophys. Chem. 2008; 132:97–103. [PubMed: 18006210]
49. Belsito S, Bartucci R, Sportelli L. Biophys. Chem. 2001; 93:11–22. [PubMed: 11604213]
50. Mazer NA, Benedek GB, Carey MC. Biochemistry. 1980; 19:601–615. [PubMed: 7356951]
51. Glover KJ, Whiles JA, Wu GH, Yu NJ, Deems R, Struppe JO, Stark RE, Komives EA, Vold RR. Biophys. J. 2001; 81:2163–2171. [PubMed: 11566787]
52. Daoud M, Cotton JP. Journal De Physique. 1982; 43:531–538.
53. Vagberg LJM, Cogan KA, Gast AP. Macromolecules. 1991; 24:1670–1677.
54. Johnsson M, Hansson P, Edwards K. J. Phys. Chem. B. 2001; 105:8420–8430.
55. Humphrey W, Dalke A, Schulten K. Journal of Molecular Graphics. 1996; 14:33–38. [PubMed: 8744570]

NIH-PA Author Manuscript

NIH-PA Author Manuscript

NIH-PA Author Manuscript

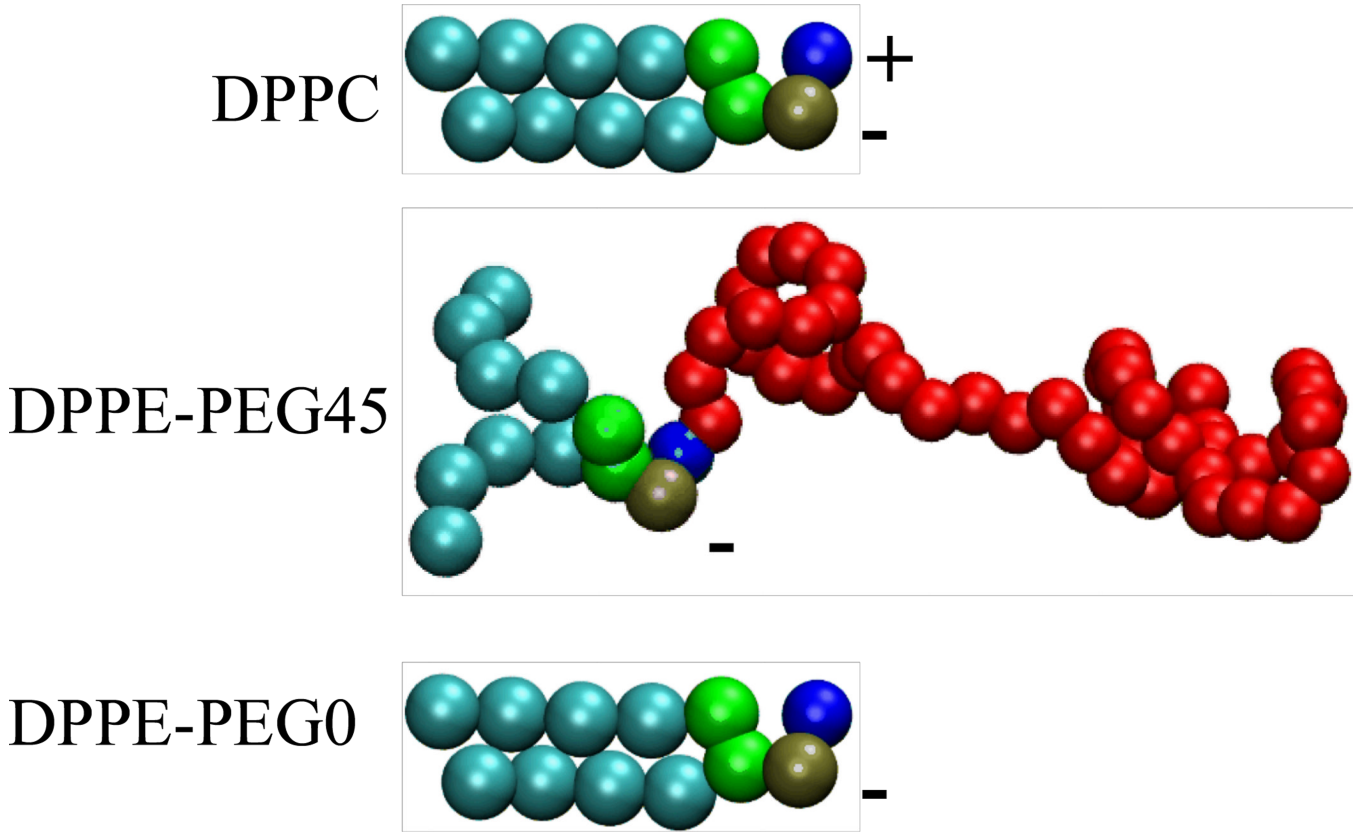

Figure 1.
Structures of DPPC, DPPE-PEG45, and DPPE-PEG0. Light blue, green, brown, blue, and red colored beads respectively represent lipid tail, glycerol, phosphate, choline, and PEG. The images were created with Visual Molecular Dynamics.[55]

NIH-PA Author Manuscript

NIH-PA Author Manuscript

NIH-PA Author Manuscript

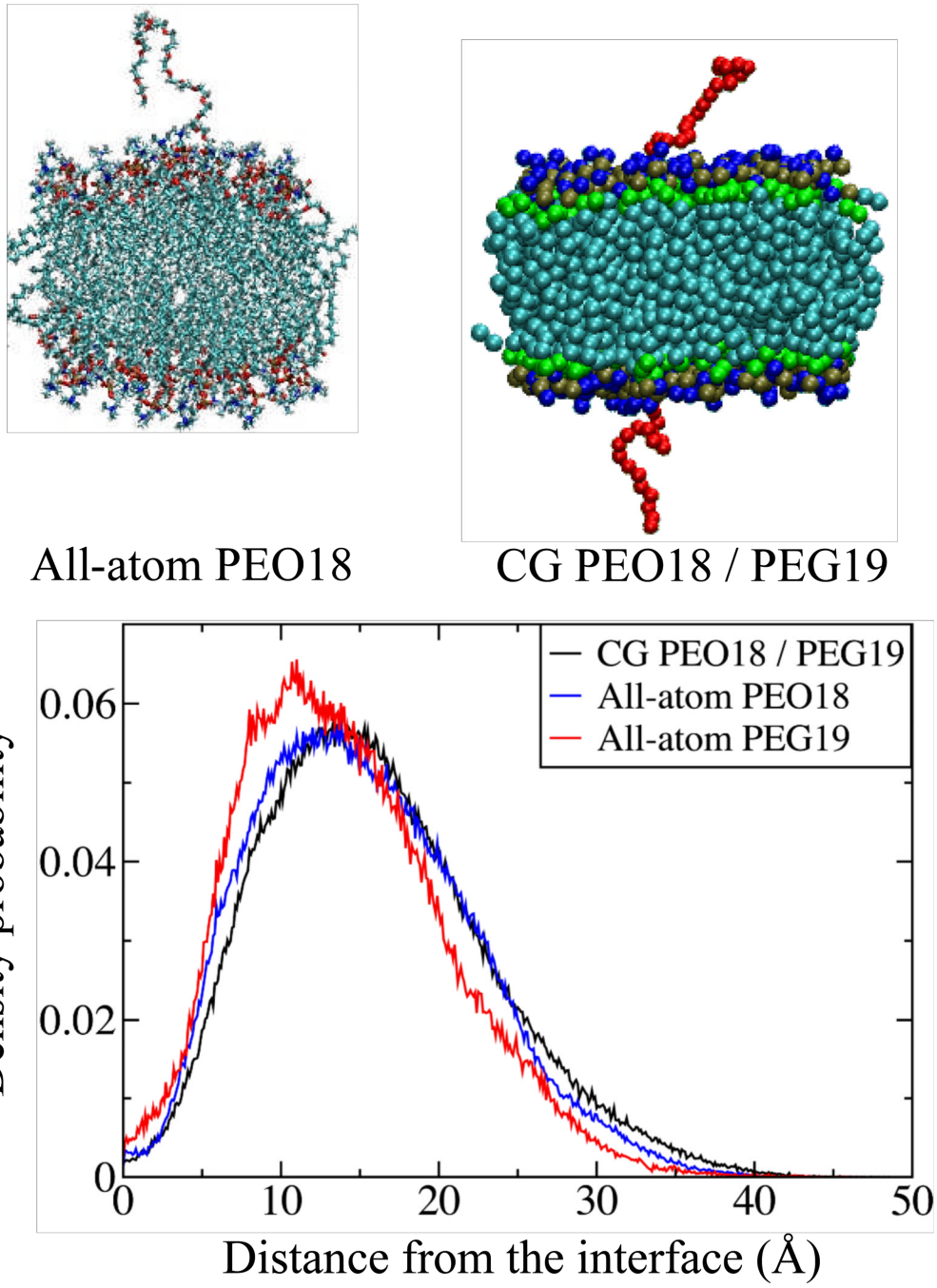

Figure 2.
Snapshots of PEO18 grafted onto DPPC lipid bilayers from all-atom (upper left) and CG (upper right) simulations. For all-atom simulations, PEO18 is attached to one leaflet, and for CG simulations PEO18/PEG19 is attached to both leaflets. Density probabilities of PEO18/PEG19 as a function of distance from the PEO/PEG-bilayer interface (bottom). The interface is defined as the average z-coordinates of the choline group.

NIH-PA Author Manuscript

NIH-PA Author Manuscript

NIH-PA Author Manuscript

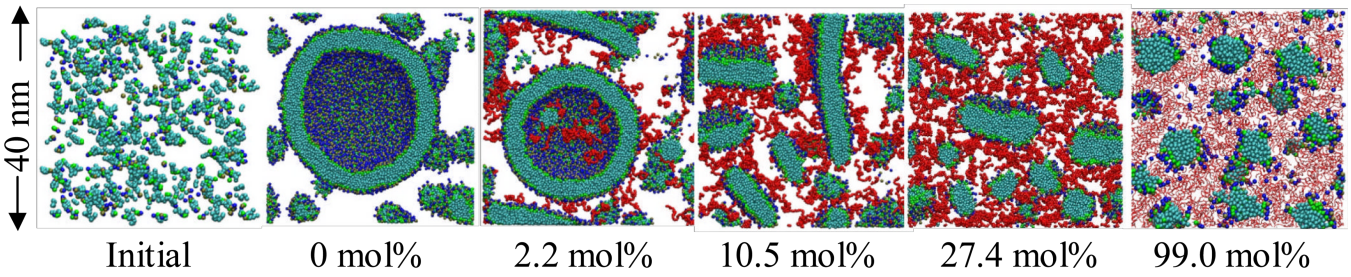

Figure 3.

Snapshots at the beginning (0 ns, *left*) and end (300 ns, columns 2, 3, 4, 5, and 6) of simulations with 0–99 mol% DPPE-PEG45. Initial configuration is shown only for a simulation with 0 mol%, but this random configuration is applied for initial configurations of all other simulations. Blue, green, and light blue dots respectively represent head groups, glycerols, tail groups of the DPPC (or DPPE) lipid, and red dots represent PEG chains. For 99 mol%, PEG chains are represented as thin red lines. For clarity, a cross section of the system is depicted, and water and ions are omitted.

NIH-PA Author Manuscript

NIH-PA Author Manuscript

NIH-PA Author Manuscript

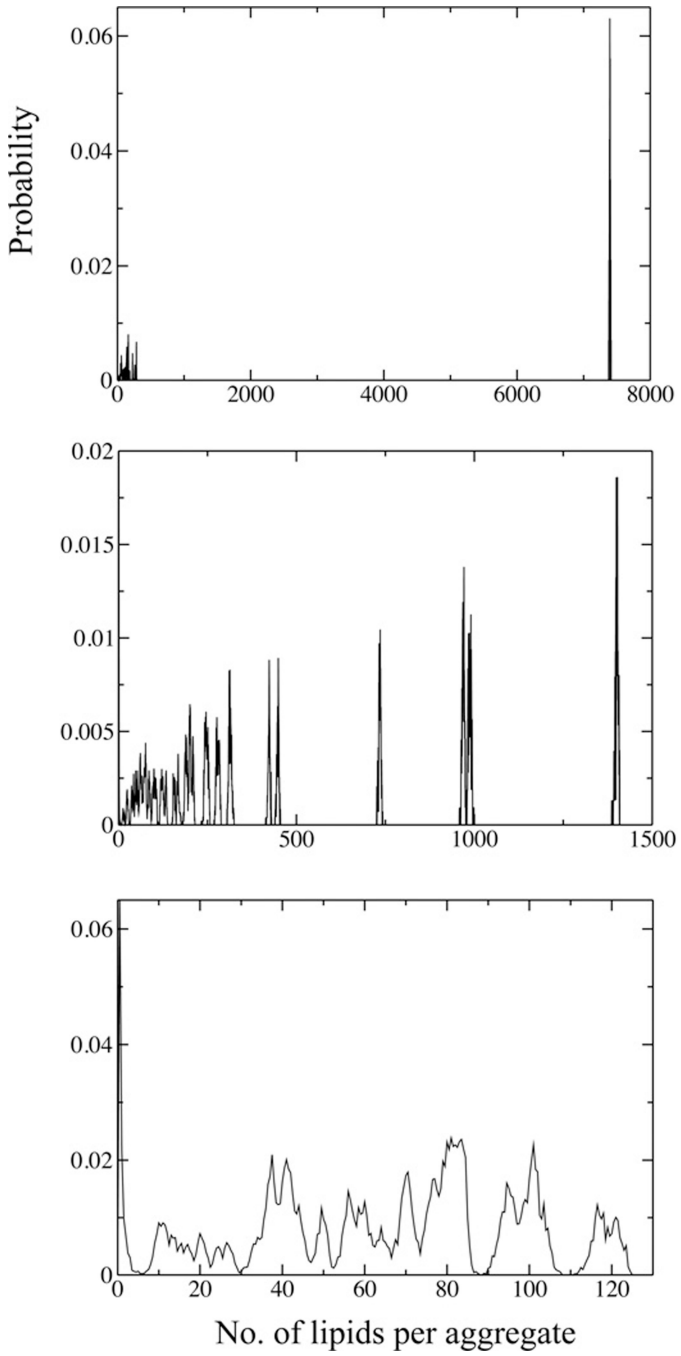

Figure 4.
Distributions of lipids per aggregate for systems with 2.2 (top), 10.5 (middle), and 99.0 mol % (bottom) DPPE-PEG45.

NIH-PA Author Manuscript

NIH-PA Author Manuscript

NIH-PA Author Manuscript

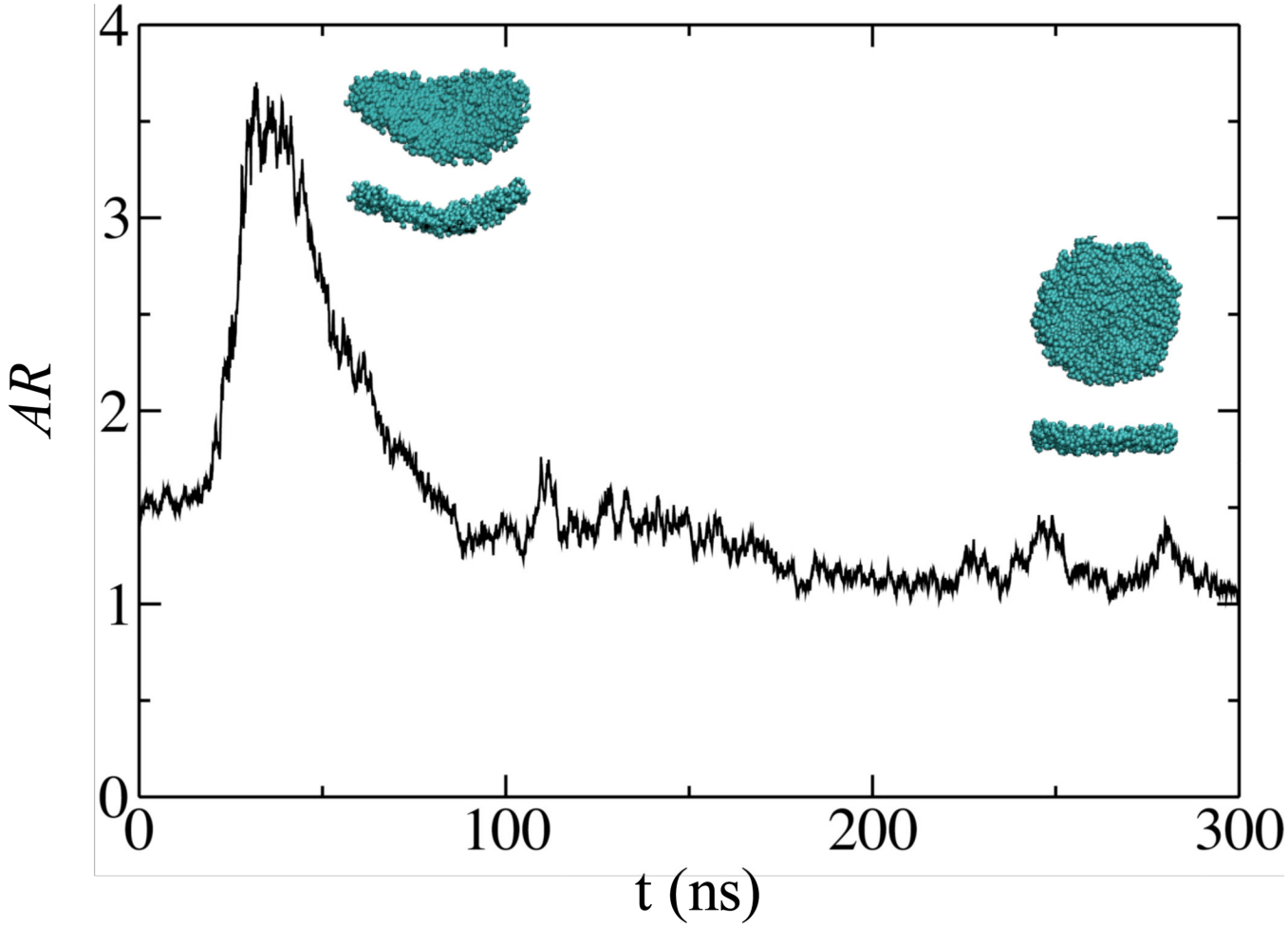

Figure 5.

Aspect ratio (*AR*) the bicelle (10.5 mol% DPPE-PEG45) calculated from principal moments of inertia as a function of simulation time. Snapshots of the top and side views of a bicelle at 30 and 300 ns are shown. For clarity, PEG chains are omitted, and only headgroups of lipids are shown.

NIH-PA Author Manuscript

NIH-PA Author Manuscript

NIH-PA Author Manuscript

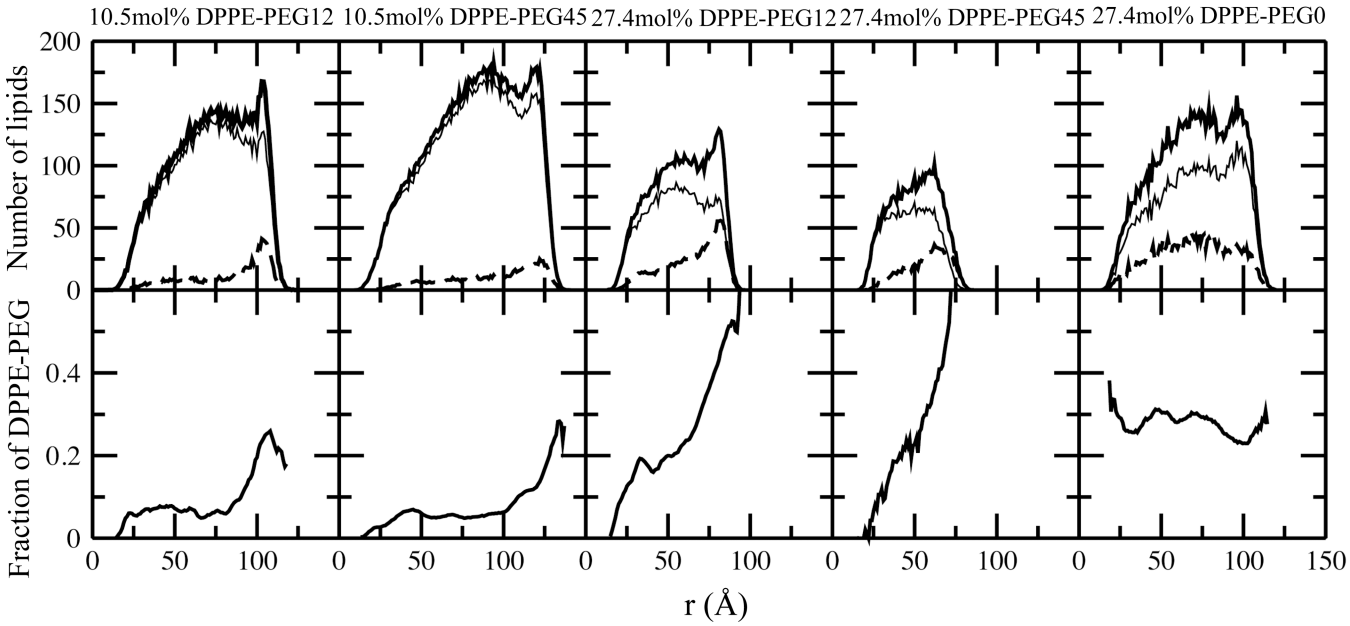

Figure 6.

The number of lipids (*top*) and fraction (*bottom*) of DPPE-PEG12, DPPE-PEG45, or DPPE-PEG0, along the radius of the bicelle (r). In the first row, a mixture of DPPC and DPPE-PEG, DPPC, and DPPE-PEG are represented as thick (▬), thin (——), and dotted line (▬ ▬), respectively.

NIH-PA Author Manuscript

NIH-PA Author Manuscript

NIH-PA Author Manuscript

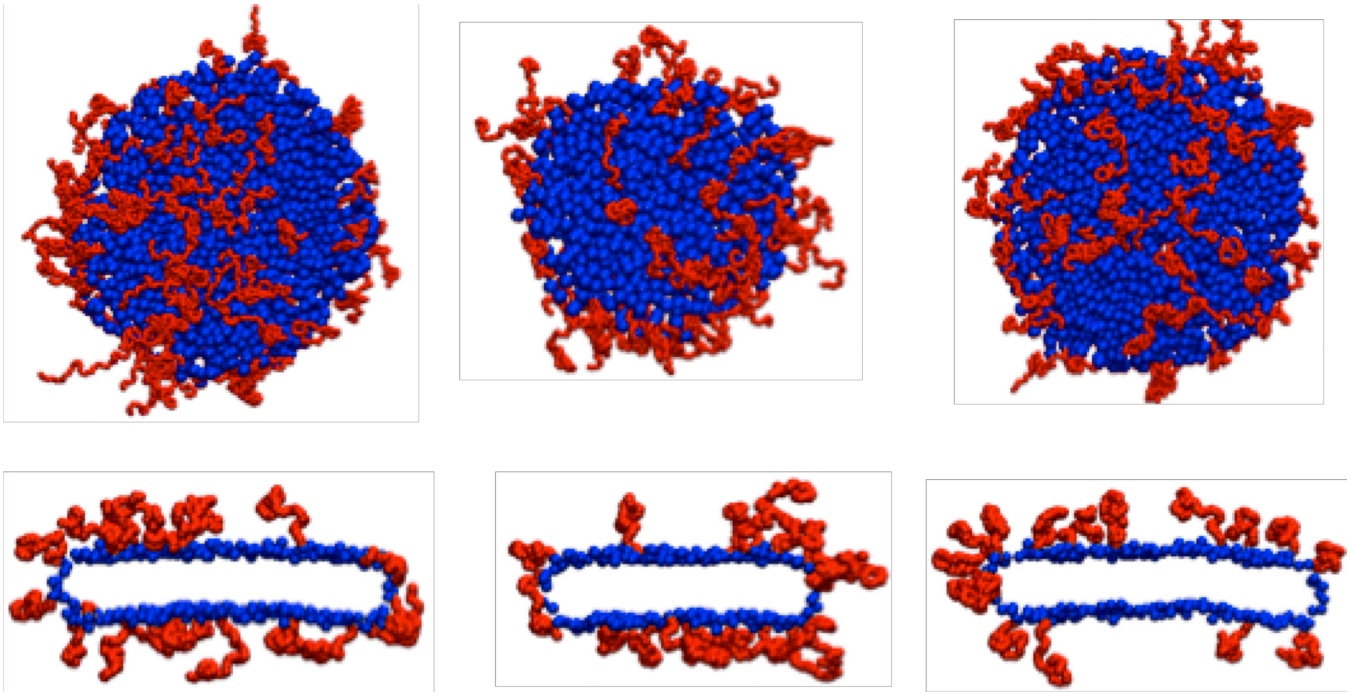

Figure 7.
Snapshots of top (*top*) and side (*bottom*) views of three bicelles at 10.5 mol% DPPE-PEG45.

NIH-PA Author Manuscript

NIH-PA Author Manuscript

NIH-PA Author Manuscript

Table 1

List of simulations. The number for each molecule in column 1 denotes the degree of polymerization for the PEG component; the molecular weight of the PEG is listed in column 2.

Name	M_w	Conc. of DPPE-PEG (mol%)	No. of lipids			No. of simulations	Length of each trajectory
			DPPC	Charged DPPE	DPPE -PEG		
DPPC	-		10500	-	-	5	300
DPPE-PEG0	-	2.2	10269	231	-	3	300
		10.5	9400	1100	-	3	300
		27.4	7625	2875	-	3	300
DPPE-PEG12	550	2.2	10269	-	231	5	300
		10.5	9400	-	1100	5	300
		27.4	7625	-	2875	3	300
DPPE-PEG28	1250	2.2	10269	-	231	5	300
		10.5	9400	-	1100	5	300
		27.4	7625	-	2875	3	300
DPPE-PEG45	2000	2.2	10269	-	231	5	300
		10.5	9400	-	1100	5	300
		27.4	7625	-	2875	3	300
		99.0	30	-	2970	1	300

NIH-PA Author Manuscript

NIH-PA Author Manuscript

NIH-PA Author Manuscript

Table 2

Number and fraction of lipids in the inner and outer layer of liposomes, and size of liposomes observed from five simulations at 2.2 mol% DPPE-PEG45.

	Number of lipids				Fraction of DPPE-PEG45		Radius (Å)	
	Inner layer		Outer layer					
	DPPC	DPPE-PEG45	DPPC	DPPE-PEG45	Inner layer	Outer layer	Inner layer	Outer layer
Liposome 1	1209	14	1946	40	0.011	0.020	70	111
2	1221	19	1945	49	0.015	0.025	71	112
3	1788	24	2643	65	0.013	0.024	86	128
4	1972	25	2833	74	0.013	0.025	91	133
5	3125	48	4234	104	0.015	0.024	117	159

NIH-PA Author Manuscript

NIH-PA Author Manuscript

NIH-PA Author Manuscript

Table 3

Number (M_n), weight (M_w), and Z-averages (M_Z) for the number of lipids per aggregate (N_{ave}), and number-average for the number of lipids in the largest aggregate (N_{max}) in simulation systems at 10.5 and 27.4 mol% DPPE-PEG.

		N_{ave}			N_{max}
		M_n	M_w	M_z	
10.5 mol%	DPPE-PEG0	352 ± 7	1367 ± 48	2550 ± 289	3130 ± 151
	DPPE-PEG12	230 ± 8	520 ± 78	811 ± 154	1193 ± 136
	DPPE-PEG28	199 ± 10	407 ± 9	643 ± 59	1035 ± 116
	DPPE-PEG45	215 ± 9	552 ± 40	896 ± 92	1324 ± 152
27.4 mol%	DPPE-PEG0	215 ± 42	422 ± 37	706 ± 125	1131 ± 191
	DPPE-PEG12	141 ± 8	228 ± 9	335 ± 12	590 ± 35
	DPPE-PEG28	94 ± 3	131 ± 3	170 ± 2	302 ± 13
	DPPE-PEG45	101 ± 4	168 ± 6	231 ± 13	439 ± 31

NIH-PA Author Manuscript

NIH-PA Author Manuscript

NIH-PA Author Manuscript

Table 4

Average root mean squared end-to-end distance $<h^2>^{1/2}$ of PEG45 molecules grafted into the surface of liposome, bicelle, and micelle. For bicelle, values were calculated separately at the edges and in the middle of the bicelle. Values for a PEG45 molecule in water and on bilayer surface are from ref. 23.

		$<h^2>^{1/2}$ (Å)
Liposome		38.8 ± 0.1
Bicelle	Edge	38.9 ± 1.6
	Middle	39.6 ± 0.7
Micelle		39.1 ± 0.1
PEG in water		36.0 ± 0.8
PEG on bilayer	50 mol% PEG	41.0 ± 1.0
	100 mol% PEG	47.0 ± 1.0